MDPI

Article

A sustainable deep learning based framework for automated segmentation of COVID-19 infected regions: Using U-Net with an attention mechanism and boundary loss function

Imran Ahmed [1], Abdellah Chehri [2] and Gwanggil Jeon [3,*]

[1] School of Computing and Information Science, Anglia Ruskin University, Cambridge, UK.
Email: imran.ahmed@aru.ac.uk.
[2] Department of Applied Sciences, University of Quebec in Chicoutimi, Québec, Canada.
Email:Abdellah$_C$*hehri@uqac.ca*.
[3,*] Department of Embedded Systems Engineering, Incheon National University, Incheon, Korea.
Email:gjeon@inu.ac.kr.

Abstract: COVID-19 has been spreading rapidly, affecting billions of people globally, with significant public health impacts. Biomedical imaging, like Computed Tomography (CT), has significant potential as a possible substitute for the screening process. Because of this, automatic segmentation of images is highly desirable as clinical decision support for an extensive evaluation of disease control and monitoring. It is a dynamic tool and performs a central role in precise or accurate segmentation of infected areas or regions in CT scans, thus, helping in the screening, diagnosing, and disease monitoring. For this purpose, we introduced a deep learning framework for automated segmentation of COVID-19 infected lesions/regions in lung CT scan images. Specifically, we adopted a segmentation model, i.e., U-Net, and utilized an attention mechanism to enhance the framework's ability for the segmentation of virus-infected regions. Since all the extracted or obtained features from the encoders are not valuable for segmentation; thus we applied the U-Net architecture with a mechanism of attention for a better representation of the features. Moreover, we applied a boundary loss function to deal with small and unbalanced lesion segmentation's. Using different public CT scan image data sets, we validated the framework's effectiveness in contrast with other segmentation techniques. Experimental outcomes showed the improved performance of the presented framework for automated segmentation of lungs and infected areas in CT scan images. We also considered both boundary loss and weighted binary cross-entropy dice loss function. The overall dice accuracy of the framework is 0.93 and 0.76 for lungs and COVID-19 infected areas/regions.

Keywords: Sustainability, Artificial Intelligence, Biomedical Images, Deep Learning, COVID-19.

Citation: Title. *Journal Not Specified* **2022**, *1*, 0.

Received:
Accepted:
Published:

1. Introduction

Coronavirus epidemic was reported in late December 2019 in Wuhan city; after its emergence, it spread rapidly worldwide [1]. It is a deadly viral infection/illness caused due to Severe Acute Respiratory Syndrome Coronavirus 2 (SARS-CoV-2). It retains several properties that make it highly contagious; therefore, enforcing people to adopt government safety and prevention measures like social distancing [2], and [3] and raising the necessity for rapid and reliable diagnosis of the infection. As far as July 2, 2022, based on the reports and statistics of the World Health Organization shown in Figure 1[1], over 545, 226, 550 people have been affected by COVID-19 infection, and 6, 334, 728 have lost their lives, around the globe. Thus, reliable and timely testing is essential to control the transmission and increase of the deadly virus.

[1] https://worldhealthorg.shinyapps.io/covid/

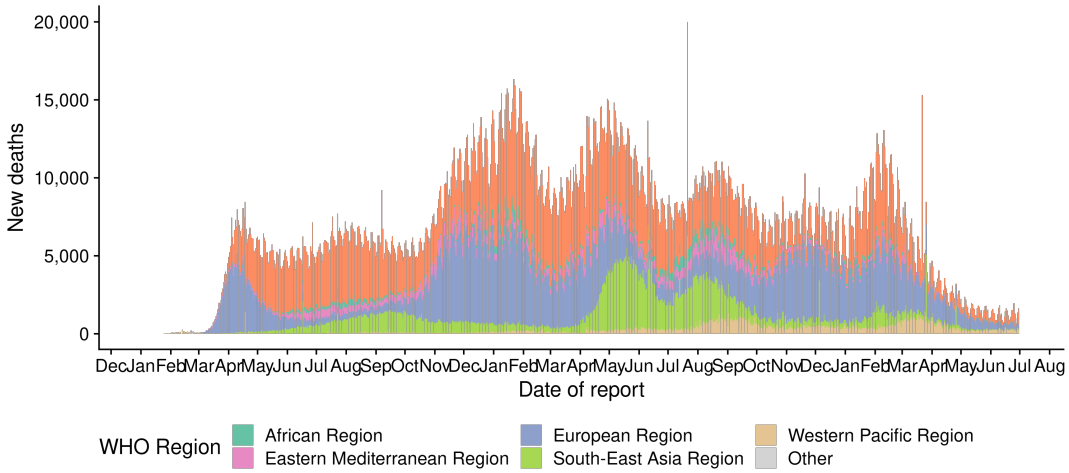

Figure 1. Recent number of confirmed cases, in different regions around the globe, from date of report, until July 2, 2022.

Biomedical image technology has been developing over the past few years as a promising tool for automatically quantifying and diagnosing different diseases. The medical image data is obtained via (magnetic resonance imaging, CT, X-ray, microscopy, and pathology) which is used to perform particularly diagnosis-oriented investigations, analyzing important diseases like human brain disorders and different kinds of cancer. Lungs and Chest CT imaging are also strongly suggested as a regular/ conventional diagnostic tool for pneumonia and is now also recommended to identify COVID-19 infection for early assessment and follow-up cases. These are very helpful in identifying common radio-graphic characteristics of COVID-19 infection [4]. Furthermore, a systematic study [5] revealed that CT images of the chest are delicate for monitoring COVID-19 even before clinical signs and symptoms are recognized. More particularly, CT scan images of patients show ground-glass opacity or bilateral patchy shadows on the infected region [6], which are usually not visible in standard X-ray images [7].

Medical specialists usually need to examine several CT scans, which is a time consuming and error-prone method. For this purpose, automated deep learning techniques are introduced in order to segment Regions of Interest (ROIs) of various sizes and shapes, for example, lungs, buds, and lesions, in high-resolution CT scan images. These techniques may help medical specialists in the diagnostic process. In literature, researchers presented various methods based on image processing, machine learning, and deep learning for automatic segmentation of CT scans [8], [9]. However, deep learning models/ techniques have surpassed feature-based methods, which have been widely and successfully used/ implemented to automatically segment ROIs in CT scan images. More particularly, applications of deep learning models/techniques [10], and [11], biomedical imaging mainly target lungs [12], lungs infections [13], pathological lungs [14], lungs and COVID-19 lesions [15]. Mostly deep learning based techniques are derived from a Fully Convolutional Networks (FCN) architecture, in which the fully connected layers are used instead of the convolutional layers [16]. The widely used U-Net model is a variant of FCN that has been developed as the de facto model for tasks of object segmentation in images because of its learnable up-convolution layers and multi-scale skip connections. [17]. Researchers used it for automatic COVID-19 lesions segmentation in CT scans.

Motivated by excellent results of deep learning architectures, we introduced an automated framework using deep learning to classify and segment deadly COVID-19 viral infection in CT scan images. We adopt a U-Net segmentation paradigm to detect and segment infected areas (regions/ lesions) in CT scans. Since all the features obtained from the encoders are not valuable; thus, we apply U-Net architecture with an attention mechanism for better feature representation. In this way, it allows highlighting of salient ROI features and control activations of features by irrelevant regions. However, the architecture faces

difficulty during balancing recall and precision due to the small ROI located in CT scan images. Thus addressing the issues of small and unbalanced data and training performance, we combined attention U-Net with the boundary loss function, which is quite fitted for small lesion segmentation. The principal contributions of the presented work are given as follows:

- To introduce a framework for automated segmentation of infected regions of COVID-19 virus in lungs/chest CT scans by using deep learning architecture.
- To utilize the soft attention mechanism in order to enhance the framework's capability, extract more silent features, and identify and segment virus-infected regions in CT scans.
- To address the issues of unbalanced data, attention U-Net architecture is combined with boundary loss function for small regions/lesion segmentation.
- To validate the effectiveness of the framework with other segmentation techniques in terms of segmentation accuracy.

The presented work in the paper is arranged as follows: an overview of different methods suggested for segmentation of infection in CT scans is presented in Section 2. Section 3 discussed the detail of the developed framework utilized for segmentation of infected regions/ lesions in CT scans images, including the U-Net architecture with attention mechanism and boundary loss function. The data set used to evaluate the framework is presented in Section 4. Furthermore, experimental results along with evaluation parameters are also addressed in Section 4. Lastly, the presented work with some future guidelines is concluded and summarized in Section 5.

2. Related Work

In an effort against COVID-19, researchers pay serious attention in order to introduce efficient and effective deep learning based techniques, for example, [18], [19], [20], [21], [22], [23], [24], [25], and [26]. These techniques are widely adopted for classification, detection, and segmentation of COVID-19 images and infection. [27], [28], and [20] used biomedical image data, mostly including Chest/lungs CT scans and X-rays in their work.

Hemdan et al., [29] applied and compared various neural network models for the classification of COVID-19 X-ray images. [30] introduced a CNN based system for analyzing and classifying three categories of X-ray images, including pneumonia, COVID-19, and regular images. Pathak et al. [31] suggested a deep learning process along with transfer learning to classify infected cases using CT scan data set. Authors in [32] studied a residual neural network model for analyzing X-rays of normal, viral, and infected pneumonia. [33] introduced convolutional neural networks based on a multi-objective differential evolving model to distinguish the coronavirus patients utilizing CT scan data of the chest. Hossain et al., [34], proposed a healthcare system using artificial intelligence to detect the virus using chest CT scans and radiology images.

Muhammad et al., [35], presented a multi-layers fusion model for the classification of COVID-19 utilizing ultrasound images of lungs. Researchers in [36] presented a neural network model using contrastive loss to detect COVID-19 in radiology pictures. Apostolopoulo et al., [37] introduced a detection system using neural networks and transfer learning to analyze chest X-rays. [38] made COVID-19 identification using their own developed data set, containing a total of 1144 radiology images. [39], adopted a Faster-RCNN, a detector model for monitoring of COVID-19 virus in X-ray images. Authors in [40] and [41] trained 2D CNN model for data set collected from [42]. [40], authors combined different pre-trained designs with regularization of the support vector machine.

In [41], researchers introduced a network by leveraging the power of capsule networks with different architectures to increase classification accuracies. Song et al., [43] produced a deep learning diagnosis framework to assist medical experts in identifying patients with symptoms of COVID-19 virus and pneumonia in CT scan data. [44] proposed a 3D deep network comprised of a pre-trained U-Net and two 3D residual blocks. [45] also used 3D deep networks for segmentation of CT images. In [46], authors used GAN incorporated

data to enhance the learning of a discriminating paradigm for diseased lung segmentation. Jiang et al., [47] produced deep neural networks for tumor segmentation in lung CT slices by combining various residual layers of modifying resolutions. In another work [48], researchers developed an explainable method for diagnosing viral infection by shared segmentation and classification approach. [49], aims to offer an automated system to segment viruses caused by COVID-19 and presented a quantitative measure of infections to medical experts. The method involves segmentation of lung segmentation infection based on U-Net architecture.

Yan et al., [13], recommended a deep neural network model called COVID-SegNet to segment infection in CT scans. A small network for the effective segmentation of the deadly viral diseases in CT scans is presented by [50]. Authors in [51] presented a U-Net based computerized model for infection segmentation in lung CT scans. Shan et al., [15], introduced a deep learning design defined as VB-Net for segmenting infection lesions in the CT scan data set. [52], studied five convolutional neural network pre-trained models for classifying and analyzing infected patients utilizing a chest X-ray data set. A deep learning model for lung disease segmentation named Inf-Net is presented by [53]. The model automatically recognizes infected regions in CT scan data. Authors used an identical partial decoder to combine the distinctive characteristics and produced a global map. To enhance the representations and the boundaries, authors applied reverse and specific edge-attention. Ahmed et al., [54] recently presented an Internet of Things (IoT) enabled deep learning model for screening of COVID-19 in X-ray images. Authors in [55], and [56], presented an automated COVID-19 CT scans segmentation method which is based on U-Net.

Researchers presented various techniques to classify, detect and segment chest or lung X-rays, CT scan images, and infected areas (regions and lesions) of COVID-19 patients. Mostly researchers adopted state-of-the-art methods and approaches to classify, analyze and differentiate contagious diseases, but they used a limited data set. This paper introduced a deep learning framework based on U-Net architecture for segmentation of COVID-19 infected lesions/regions in chest/lung CT scan data set. In addition to segmentation, the developed framework can also highlight the severity of the disease in CT scans.

3. Methodology

This work introduced an automated framework using deep learning for the segmentation of infected regions/areas in the COVID-19 CT scan image data set. The framework provides a classification of viral infections and assists medical experts in order to analyzing the severity of infection. The overall technical flow of the designed framework is explained in Figure 2. The method involves five steps: pre-processing, data augmentation, lung segmentation, infection segmentation, and infection classification. The data sets used for experimentation are collected from different available online resources.

A widely utilized deep learning model named U-Net is utilized to segment lungs and infected areas. Data normalization is performed during the pre-processing step, and the input image pixel values are converted in the range [0.1], ensuring that all input pixels have the same data distribution. This increases convergence while training the network. Moreover, data augmentation is applied, e.g., random scaling, brightness, rotation, crop, contrast, and flip. Data augmentation enables the deep learning network to learn a wide variety of variations in the given data set and enhance the framework's performance. In order to learn target features of varying shapes and sizes, the U-Net architecture is combined with an attention mechanism.

In addition, a boundary loss function and integrals interface between ROIs are applied to decrease the complexity of unbalanced areas. After segmentation, different metrics are estimated to quantify the infected areas, like volumes of an infected region or regions within the lungs. Additionally, to estimate the severity of diseases and the spread of viral infection in the lungs, the percentage of infection in the lungs is determined. For that reason, we used the Hounsfield unit, histogram of the infected area to envision Ground Glass Opacification/opacity (GGO), and consolidation segments inside the infected region.

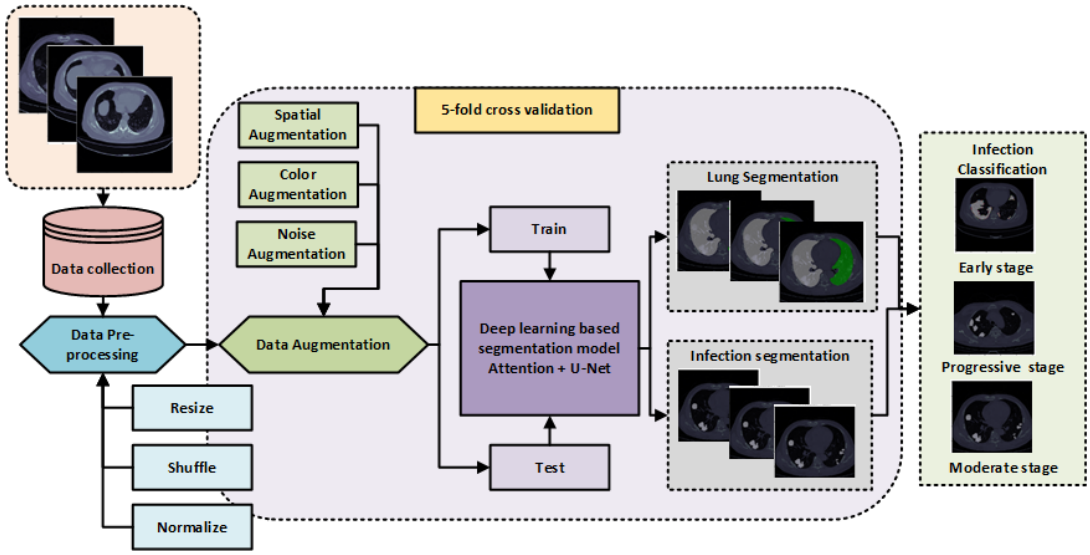

Figure 2. General flow chart of the framework developed for biomedical image examination of COVID-19 infection found in CT scans of chest/lungs. The workflow starts with the collection of the data set, the pre-processing step, data augmentation, and train/test split. In addition, the U-Net model is utilized for lung segmentation and infection in CT images. Finally, the detected infection mask is classified into three stages, i.e., early, progressive, and severe. The flowchart concludes with the estimated results of the assessment for a 5-fold cross-validation.

3.1. Pre-processing and Data Augmentation

As the data set collected from different resources is limited thus, data augmentation is performed. Its purpose is to generate large data on acceptable modifications of the needed configuration and artificially increases the amount of training images. We conducted extensive data augmentation and made an increase in data by utilizing the batch generators interface inside MIScnn [2]. We executed three kinds of augmentations: first one is the spatial augmentation, which involves (rotations, mirroring, scaling, and elastic deformations), color augmentation (contrast, brightness, and gamma adjustments), and noise augmentations. After performing pre-processing and data augmentation, the data set images are randomly splitted into training and testing samples.

3.2. Lungs and Infection Segmentation using U-Net with attention mechanism

For segmentation of lungs and infected areas in CT scan images, we applied the U-Net model. [17] introduced this model that is practically developed using end-to-end fully convolutional networks rather than dense layers. The general design of the model is presented in Figure 3 (adopted from [17]); it can be seen that the model can handle arbitrary/variable size images. The overall model is basically divided into two parts, namely encoder and decoder. The first part is used to get the context of the image, which is named an encoder. This part is mainly based on a traditional pile of convolutional layers followed by max-pooling layers. In contrast, the other part is the symmetric/ balanced expanding path named decoder is used to provide accurate localization using transposed or reversed convolutions. The first part is also named the downsampling path, which implements various classification models as the backbone. All step generally uses two convolution layers (3×3) with batch normalization followed by a max-pooling layer (2×2), as illustrated in Figure 3. The parallel bottleneck contains two convolution layers and up convolution layers of size (3×3) and (2×2), respectively. The upsampling path has four phases, the decoder with two convolutional layers followed by an upsampling layer of size 3×3 and 2×2, respectively. The feature maps become half after each step.

[2] https://github.com/MIC-DKFZ/batchgenerators

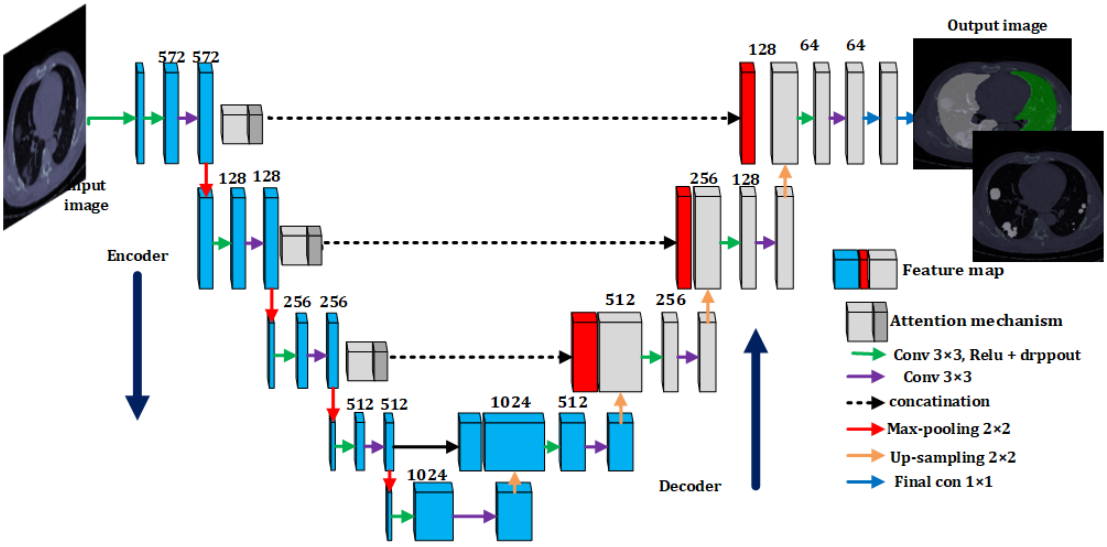

Figure 3. U-Net architecture with attention mechanism utilized for segmentation of lungs and COVID-19 infected virus.

From Figure 3, it can be observed that to produce global and local information throughout upsampling. The architecture skips connections within downsampling and upsampling paths. The pre-processed input images with 3-channel are provided to the architecture for segmentation. Finally, the segmented map is given, using a convolutional layer of 1×1 at the output. The extracted feature maps are of identical size to desired output segments. Thus, a function is defined over the absolute feature map with pixel-wise soft-max and cross-entropy loss as [17]. It is described as follows;

$$p_k(x) = \frac{exp(a_k(x))}{\sum_{k'=1}^{K} exp(a'_k(x))} \tag{1}$$

In Equation.1, ReLu is an activation function (Rectified Linear Unit) used for feature maps and it is defined as a_k. The number of classes are represented with K, and approximation for maximum value is represented as $p_k(x)$. For maximum $a_k(x)$, its value is approximately equal 1, and considered as $p_k(x) \approx 0$ for other values. The function defined in Equation.1 is penalized and given as [17];

$$E = \sum_{w(x)\epsilon\Omega} \log(p_{l(x)}(x)) \tag{2}$$

In Equation.2, true label or ground truth of all pixels is described as $l : \Omega \rightarrow 1, 2, ..., K$. The weight map that is used throughout training for additional attention to pixels is provided as $w : \Omega \rightarrow \mathbb{R}$ [17]. For various frequency pixels, the true segmentation is precalculated. Applying morphological operations for different classes in the training data set; the weight map value is estimated as follows;

$$w(x) = w_c(x) + w_o.exp\left(\frac{-(d_1(x) + d_2(x))^2)}{2\sigma^2}\right) \tag{3}$$

Therefore, the weight map used for balancing frequencies of different classes is represented with $w_c : \Omega \rightarrow \mathbb{R}$. The distance value between the initial edge and second nearby edge is denoted with d_1 and d_2. The value of w_o is set to 10 and $\sigma \approx 5$. (Readers are referred to the actual work [17] for more details)

During upsampling, the recreated spatial information in the expanding path lack accuracy. To counter this issue, the U-Net applies to skip connections that integrate spatial information from the down sampling path to the upsampling path. However, this causes

several unnecessary extractions of low-level features, as feature description is not good in the primary layers. Thus, the attention mechanism is implemented or applied at the skip connections, vigorously overcoming activations in inappropriate areas or regions and decreasing redundant features.

The attention gates introduced by [57] use additive soft attention as shown in Figure 4. These gates take two input vectors that are represented as x and g. The vector, g, is obtained from the following lowest/deepest layer of the network. It has improved feature description and small dimensions. In Figure 4 vector x has $64 \times 64 \times 64$ (height x width x filters) and vector g has $32 \times 32 \times 32$ dimensions. The x and g pass through a strided convolution and 1×1 convolution layers, respectively, such that their dimensions become $64x32x32$. The two vectors are added element-wise, resulting in aligned weights being more extensive while unaligned weights are becoming comparatively smaller.

The resultant output vector is passed through a activation layer ReLU, and a convolution layer of 1×1 that drops the dimensions to $1 \times 32 \times 32$. Moreover, it passes within a sigmoid layer, which computes the vector in the range of [0,1], providing the weights (attention coefficients), where coefficients nearer to 1 exhibit more important characteristics. These coefficients are also up-sampled to the real dimensions 64×64 of the x utilizing the trilinear interpolation. Next, element-wise multiplication of the attention coefficients is performed to the real x, scaling the vector according to their significance and crossing along in the skip connection as usual.

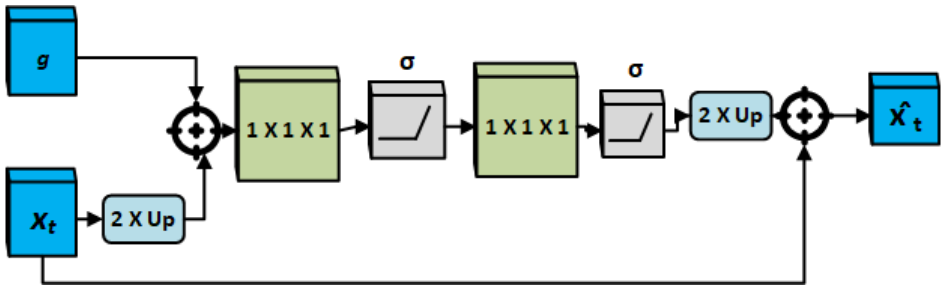

Figure 4. Schematic design of additive attention gate used in attention mechanism. Input features x are estimated with coefficients σ to develop important features for the output of the $\hat{x}$ (decoding layer). The spatial gating g signal gives contextual knowledge, while spatial fields from the x input are location information. Bilinear interpolation is used for feature map re-sampling.

In this work, we used a boundary loss function that applies a distance metric on the shapes or contours instead of considering whole areas or regions [58]. The boundary loss is highly used for unbalanced segmentation tasks. In this way, it tackles the difficulties posed by local losses for highly unbalanced segmentation tasks. The boundary loss function is defined as;

$$Dist(\partial G, \partial S) = \int_{\partial G} ||y_{\partial G}(p) - p||^2 dp \tag{4}$$

In above equation, $p \epsilon \Omega$, where Ω is a limit on boundary at specific region ∂G and $y_{\partial G}(p)$ shows the corresponding boundary point ∂S, and the normal direction to ∂S as shown in Figure 4. $y_{\partial G}(p)$ represents intersection of ∂S and the line, normal to ∂S at p . $||$ represents the L2 norm. (For more information about the boundary loss function we refer reader to [58]).

3.3. Classification of infection severity

After segmentation of the lungs and infection area (regions/lesions) in the CT scan data set, the severity of the viral infection needs to be analyzed. The infected areas are described as air space consolidation and ground-glass opacity, or complete opacity. Their level of concentration observed in lung and infected regions/lesions assists in determining the different stages of the severity of infection. In the initial stage, the appearance of

ground-glass opacity is usually found in one or different shapes, like in the form of a fine mesh or shadow/cloud of light. Infrequently, the concentration is found near the bunches of blood vessels (bronchial) or under the pleura. In the progressive stage, the GGO/shadows increase, or the infected region expands, starting to absorb, therefore resulting in consolidation at a large scale. Finally, in the critical or severe stage, the consolidation of the bilateral or unilateral lungs diffuses, identified by GGO and symptoms of the bronchial disease.

In the diffusion or absorption step, the primary regions/ lesions are entirely absorbed and grown. Therefore, to control the severity of the viral infection in the lungs (the proportion between the size of the infected area and lungs), it is essential to estimate the degree of concentration/consolidation of the infected regions. Therefore, sub-areas of these segmented lesions are categorized as consolidated in case the voxel intensity is more prominent than 0 Hounsfield units (HU), and else, it is categorized as GGO [7], [59]. Therefore, it is reasonable to estimate the variation in the concentration of the lesions caused by a viral infection, e.g., COVID-19. Figure 2 presents an illustration of the classification of infected regions into three different stages of severity. In addition, the results of infection severity classified in lung CT scans are shown in Section.4.

4. Experimental Results

Experimentation of the above-discussed model is presented in this section. Firstly, we discussed training and testing observation—secondly, the output results of the segmentation model employed for monitoring and screening of viral COVID-19 infection in CT scan images. Finally, the model evaluation results are discussed, showing the model's performance. The introduced framework has been implemented using a python programming language (Keras library) with OpenCV 3.6.

4.1. COVID-19 CT scan data set

The data sets utilized in the experiments are collected from different online repositories e.g., COVID-19 CT scans from Italian Society of Medical and Interventional Radiology [3], [4] and [5]. More than 800 CT scans of patients suffering from COVID-19 have been obtained from these sources. The data set includes CT scans of diagnosed patients with viral infection and lung segmentation and infections analyzed by experts. The size of images is 512×512 pixels. The images have been resized, grey scaled, and compiled into a separate NIFTI file. Images are segmented by radiologists utilizing three labels: consolidation, ground-glass, and pleura effusion. The total number of training and testing CT scan slices used for experimentation after data augmentation and pre-possessing is provided in Table 1.

Table 1. Description of data set used for experimentation.

S.No	Images	COVID-19	Non-COVID-19	Total
1	Training Slices	800	1000	1800
2	Testing Slices	200	1200	1400
3	Total	1000	2200	3200

4.2. Training and Validation

These observations, including training and validation loss and accuracy curves of the above discussed segmentation architecture with attention mechanism, are illustrated in Figure 5. Training of the model is performed for 100 epochs. It has been observed that after the 10^{th} epoch, the loss values decline for training and validation. Both values are contrasted in Figure 5. During training, when validation is performed, no over-fitting is

[3] https://sirm.org/category/senza-categoria/covid-19/
[4] https://radiopaedia.org/playlists/25887
[5] http://medicalsegmentation.com/covid19/

noted, showing no notable difference between them. While the validation performance is settled down during fitting, at a loss value of around 0.3, and the training performance is 0.2. Due to the robust training method externally, without any implications of over-fitting, we determined that adapting randomly generated patches using increased data and arbitrary cropping from varying data sets is very effective for limited image data. As a result, the overall loss values after the 10^{th} epoch are improved to 0.89. In Figure 5, we show the training and validation accuracy of the model during training, which is 0.99 at the end of the 20^{th} epoch.

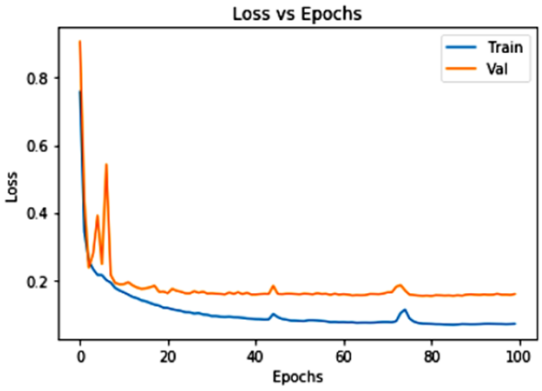

(a)

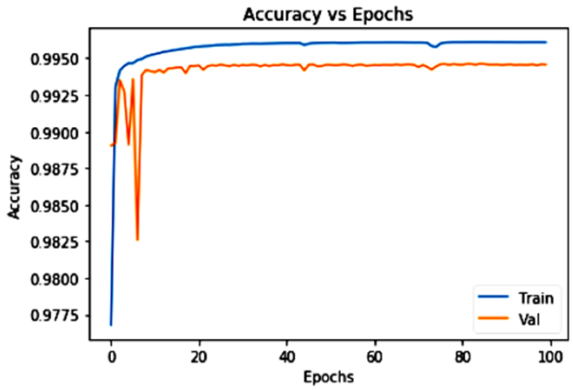

(b)

Figure 5. (a) Loss curve during the validation and training process. (b) Accuracy curve during the validation and training process for training. The lines [validation (orange) and training (blue)] are estimated using binary cross-entropy dice loss and represent the weight loss across all folds.

4.3. Visualization results of infected regions segmentation

The segmentation and classification results of the segmentation framework are illustrated in Figure 6. We can see that the segmentation model effectively segmented the infection regions in CT scans. It can also be observed that the boundary loss function improves the segmentation results of unbalance regions or data. In Figure 6(a) and Figure 6(b), we demonstrate the example results of infection segmentation at an early stage of diagnosis. It can be seen that the segmented regions are so small and cannot be easily analyzed in original CT scans. While all small spots of segmented infection using the above model might help medical experts to effectively analyze and diagnoses the virus at its earlier stages.

Similarly, in Figure 9(c) and Figure 9(d), we show the output results for progressive stages; it can be seen from the images that the virus is growing at different places irregularly;

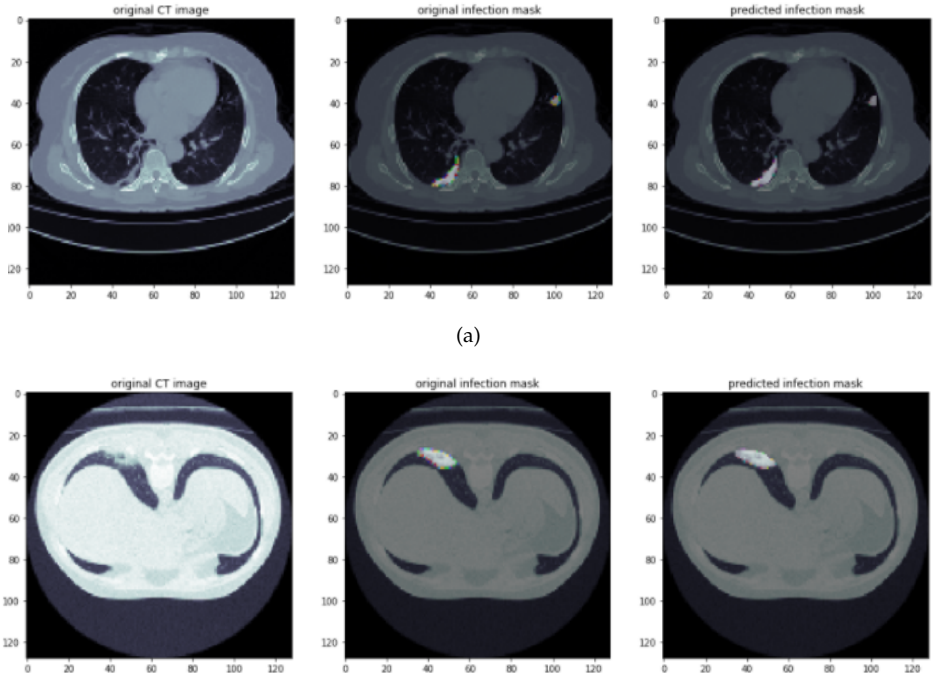

(a)

(b)

Figure 6. Infection segmentation results of CT scans, the sample images shows the early stage of viral infection. Columns 1 to 3 shows Original CT scan image, original infection mask, and predicted infection mask, respectively.

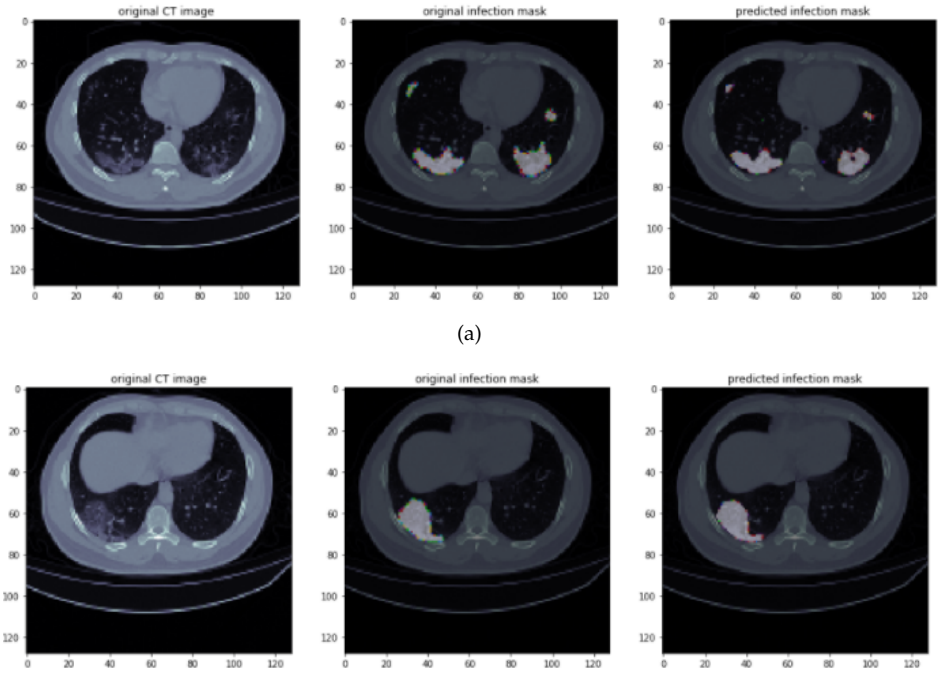

(a)

(b)

Figure 7. Infection segmentation results of CT scans, the sample images shows the progressive stage of viral infection. It can be seen that both lungs are affected from the virus, and infection is growing at different locations of lungs. Columns 1 to 3 shows Original CT scan image, original infection mask, and predicted infection mask, respectively.

at different locations in lungs. Such output results also help to analyze the progressive rate of the viruses. Moreover, along with the large regions, a small art is detected.

Figure 8(e) and Figure 8(f) we have shown the output results for the severe stage of the infected virus. As can be seen in the example images, the virus badly affected the lungs of the patients. In both sample Figures, it can be observed that the growth of infection is severe in both lungs and is spreading badly in the lungs of the patients. The results of the segmentation models can be really useful for medical specialists in order to analyze the effect of the virus on patients' lungs.

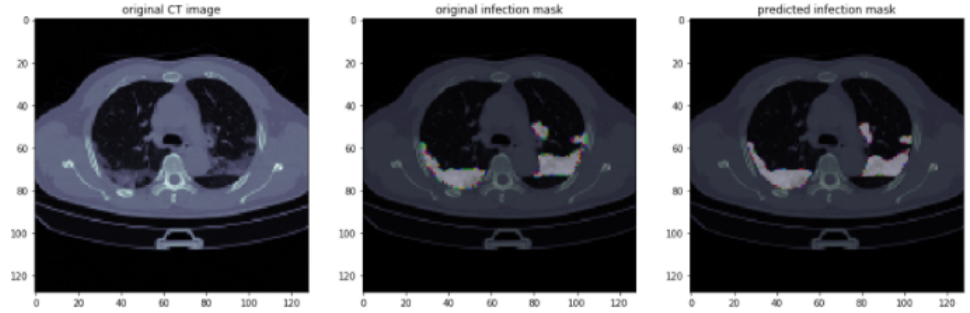

(a)

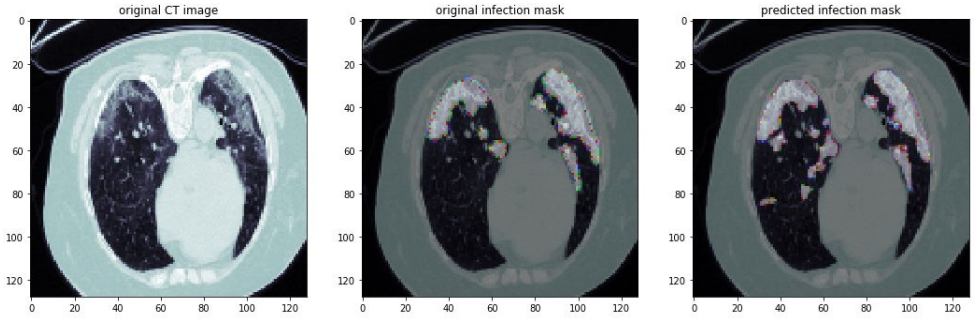

(b)

Figure 8. Infection segmentation results of CT scans, sample images show the severe stage of viral infection. It can be seen that, both lungs are badly affected from COVID-19 infection. Columns 1 to 3 shows Original CT scan image, original infection mask, and predicted infection mask, respectively.

4.4. Evaluation and Comparison results

After training and validation, we used three commonly adopted evaluation parameters for biomedical image investigations. First, to perform performance analysis to determine the overlap of segmentation between prediction and true labels/ground truth, we used the Dice similarity coefficient, described in Equation 5. It is the most widely applied parameter in segmentation applications. In addition, specificity and sensitivity discussed in Equation 6 and Equation 7 are also applied in the most popular pharmaceutical fields. All parameters are calculated using the confusion matrix, including True Positive (TP), True Negative (TN), False Positive (FP), and False Negative (FN).

$$Dice = \frac{2 \times TP}{2TP + FP + FN} \tag{5}$$

$$Specificity = \frac{TN}{TN + FP} \tag{6}$$

$$Sensitivity = \frac{TP}{TP + FN} \tag{7}$$

We determined the evaluation parameters in the cross-validation for each fold and, therefore, for all CT images in the collected data set. Overall, the cross-validation of the segmentation model obtained a *Dice* similarity coefficient of around 0.93 for lungs and 0.76 for infected regions segmentation, as depicted as box plots in Figure 9.

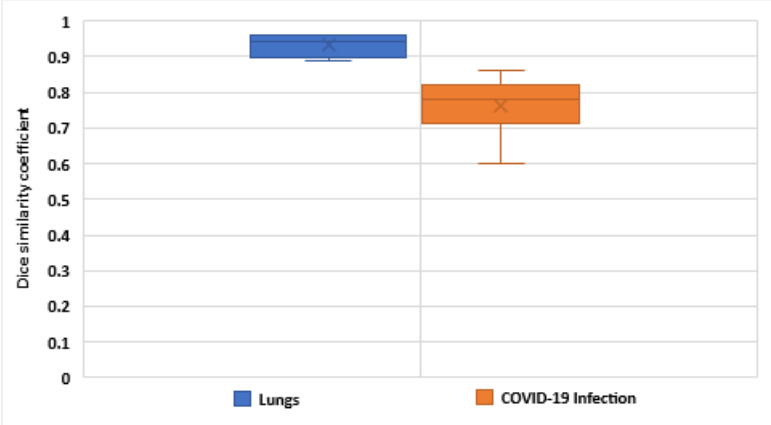

Figure 9. Result distribution of 5-fold cross-validation is presented using box plots for lung and infected region segmentation.

The average performance values of the above discussed segmentation model are shown in Figure 10. The segmentation model delivers an average rate of 0.932, 0.936, and 0.946, Dice similarity coefficient, Sensitivity, and Specificity for lung segmentation, respectively. While for COVID-19 infected regions segmentation, the Dice similarity coefficient, *Sensitivity*, and *Specificity* are 0.764, 0.736, and 0.888, respectively.

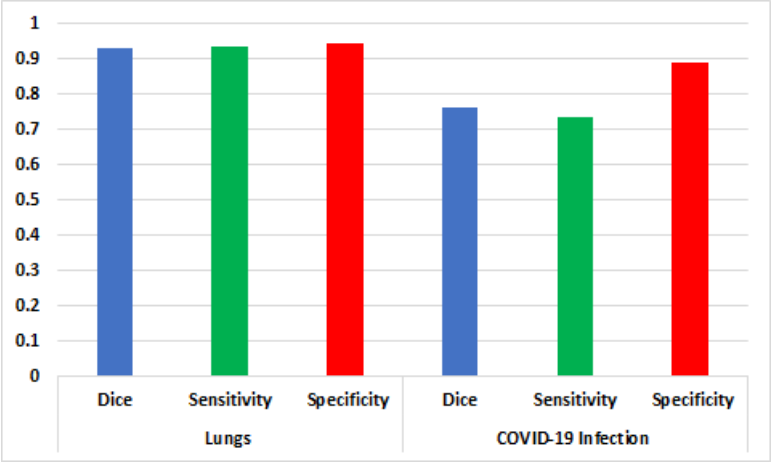

Figure 10. Average values of *Dice* similarity coefficient, *Sensitivity* and *Specificity*.

The inference performance details for each fold during cross validation are listed in Table 2. From a medical perspective, segmentation of infected regions is a difficult task and one reason for the lower value of segmentation accuracy as corresponded to the accuracy results of segmentation of the lungs. The infer for this may be the difference between pulmonary consolidation and GGO morphology. Although, our deep learning based segmentation model obtained considerably good results and segmented COVID-19 infected regions with state-of-the-art efficiency comparable to other segmentation techniques.

Table 3 presents the comparative analysis of different methods used to segment COVID-19 infection in lungs CT Scan images. The U-Net [17] model achieves an average accuracy of 0.966, while the attention U-Net [60] obtained average accuracy is 0.978. Other two segmentation model also achieve good accuracy results as U-Net++ [61], and SD-UNet [62] accuracy is 0.971 and 0.981 respectively. Our proposed model shows excellent

Table 2. Obtained results for each cross-validation fold.

Fold	Lungs			COVID-19 Infection		
	Dice Similarity	Sensitivity	Specificity	Dice	Sensitivity	Specificity
1	0.89	0.9	0.95	0.6	0.57	0.92
2	0.9	0.96	0.96	0.8	0.87	0.93
3	0.96	0.94	0.95	0.81	0.89	0.89
4	0.95	0.95	0.95	0.75	0.55	0.8
5	0.96	0.93	0.92	0.86	0.8	0.9
Average	0.932	0.936	0.946	0.764	0.736	0.888

results as we apply the boundary loss function. As discussed earlier, highly unbalanced segmentations, like regional summations where values are different in magnitude across types, affect training stability and performance. Thus, we applied a boundary loss, which uses the distance metric on the area of contours, not regions. Furthermore, it might mitigate the highly unbalanced problems by utilizing integrals instead of unbalanced integrals over the interface between regions. We can see the results from Table 3, as the *Dice* similarity of our proposed model is 0.763, higher than other methods.

Table 3. Comparison analysis of different segmentation methods.

S.No	Methodology	Average Dice Similarity	Average Accuracy
1	U-Net [17]	0.563	0.966
2	Attention U-Net [60]	0.507	0.978
3	U-Net++ [61]	0.586	0.971
4	SD-UNet [62]	0.593	0.981
5	Ours Attention U-Net with boundary loss function	0.763	0.982

5. Conclusion and Future Directions

This work introduced an automated framework using deep learning for segmentation of infected regions/lesions/areas of the COVID-19 virus in the CT scan data set. We adopted a U-Net model for segmenting lungs and infected regions of the virus and employed the soft attention mechanism to increase the framework's ability. Moreover, we performed pre-processing and extensive data augmentation to improve the segmentation model's accuracy. Furthermore, a boundary loss function is used to deal with small and unbalanced lesions or regions segmentations. We validated the framework's effectiveness in contrast with other segmentation techniques with publicly available CT image data sets. Experimental outcomes show the excellent performance of our framework for automated segmentation of lungs and infected in chest/lungs CT scan images. We also consider both boundary loss and weighted binary cross-entropy dice loss functions. The overall accuracy of the framework is 0.93 and 0.76 for lung segmentation and infected regions segmentation, respectively. In the future, this work might be extended to analyze and segment other viral infections; we might use other segmentation techniques based on deep learning applications to analyze, detect, and classify different viral diseases.

References

1. Zhu, N.; Zhang, D.; Wang, W.; Li, X.; Yang, B.; Song, J.; Zhao, X.; Huang, B.; Shi, W.; Lu, R.; et al. A novel coronavirus from patients with pneumonia in China, 2019. *New England journal of medicine* **2020**.
2. Ahmed, I.; Ahmad, M.; Rodrigues, J.J.; Jeon, G.; Din, S. A deep learning-based social distance monitoring framework for COVID-19. *Sustainable Cities and Society* **2021**, *65*, 102571.
3. Ahmed, I.; Ahmad, M.; Jeon, G. Social distance monitoring framework using deep learning architecture to control infection transmission of COVID-19 pandemic. *Sustainable Cities and Society* **2021**, *69*, 102777.

4. Li, Y.; Xia, L. Coronavirus disease 2019 (COVID-19): role of chest CT in diagnosis and management. *American Journal of Roentgenology* **2020**, *214*, 1280–1286.
5. Salehi, S.; Abedi, A.; Balakrishnan, S.; Gholamrezanezhad, A. Coronavirus disease 2019 (COVID-19): a systematic review of imaging findings in 919 patients. *American Journal of Roentgenology* **2020**, *215*, 87–93.
6. Wang, D.; Hu, B.; Hu, C.; Zhu, F.; Liu, X.; Zhang, J.; Wang, B.; Xiang, H.; Cheng, Z.; Xiong, Y.; et al. Clinical characteristics of 138 hospitalized patients with 2019 novel coronavirus–infected pneumonia in Wuhan, China. *Jama* **2020**, *323*, 1061–1069.
7. Ng, M.Y.; Lee, E.Y.; Yang, J.; Yang, F.; Li, X.; Wang, H.; Lui, M.M.s.; Lo, C.S.Y.; Leung, B.; Khong, P.L.; et al. Imaging profile of the COVID-19 infection: radiologic findings and literature review. *Radiology: Cardiothoracic Imaging* **2020**, *2*, e200034.
8. Ahmed, I.; Ahmad, M.; Khan, F.A.; Asif, M. Comparison of Deep-Learning-Based Segmentation Models: Using Top View Person Images. *IEEE Access* **2020**, *8*, 136361–136373.
9. Bizopoulos, P.; Vretos, N.; Daras, P. Comprehensive Comparison of Deep Learning Models for Lung and COVID-19 Lesion Segmentation in CT scans. *arXiv preprint arXiv:2009.06412* **2020**.
10. Ahmed, I.; Jeon, G.; Chehri, A.; Hassan, M.M. Adapting Gaussian YOLOv3 with transfer learning for overhead view human detection in smart cities and societies. *Sustainable Cities and Society* **2021**, *70*, 102908.
11. Ahmed, I.; Jeon, G.; Piccialli, F. A Deep Learning-based Smart Healthcare System for Patient's Discomfort Detection at the Edge of Internet of Things. *IEEE Internet of Things Journal* **2021**.
12. Skourt, B.A.; El Hassani, A.; Majda, A. Lung CT image segmentation using deep neural networks. *Procedia Computer Science* **2018**, *127*, 109–113.
13. Yan, Q.; Wang, B.; Gong, D.; Luo, C.; Zhao, W.; Shen, J.; Shi, Q.; Jin, S.; Zhang, L.; You, Z. COVID-19 chest CT image segmentation–a deep convolutional neural network solution. *arXiv preprint arXiv:2004.10987* **2020**.
14. Harrison, A.P.; Xu, Z.; George, K.; Lu, L.; Summers, R.M.; Mollura, D.J. Progressive and multi-path holistically nested neural networks for pathological lung segmentation from CT images. In Proceedings of the International conference on medical image computing and computer-assisted intervention. Springer, 2017, pp. 621–629.
15. Shan, F.; Gao, Y.; Wang, J.; Shi, W.; Shi, N.; Han, M.; Xue, Z.; Shen, D.; Shi, Y. Lung infection quantification of COVID-19 in CT images with deep learning. *arXiv preprint arXiv:2003.04655* **2020**.
16. Long, J.; Shelhamer, E.; Darrell, T. Fully convolutional networks for semantic segmentation. In Proceedings of the Proceedings of the IEEE conference on computer vision and pattern recognition, 2015, pp. 3431–3440.
17. Ronneberger, O.; Fischer, P.; Brox, T. U-net: Convolutional networks for biomedical image segmentation. In Proceedings of the International Conference on Medical image computing and computer-assisted intervention. Springer, 2015, pp. 234–241.
18. Zhou, T.; Dong, Y.; Lu, H.; Zheng, X.; Qiu, S.; Hou, S. APU-Net: An Attention Mechanism Parallel U-Net for Lung Tumor Segmentation. *BioMed Research International* **2022**, *2022*.
19. Ahmad, M.; Ahmed, I.; Khan, F.A.; Qayum, F.; Aljuaid, H. Convolutional neural network–based person tracking using overhead views. *International Journal of Distributed Sensor Networks* **2020**, *16*, 1550147720934738. https://doi.org/10.1177/1550147720934738.
20. Shi, F.; Wang, J.; Shi, J.; Wu, Z.; Wang, Q.; Tang, Z.; He, K.; Shi, Y.; Shen, D. Review of artificial intelligence techniques in imaging data acquisition, segmentation and diagnosis for covid-19. *IEEE reviews in biomedical engineering* **2020**.
21. Wynants, L.; Van Calster, B.; Bonten, M.M.; Collins, G.S.; Debray, T.P.; De Vos, M.; Haller, M.C.; Heinze, G.; Moons, K.G.; Riley, R.D.; et al. Prediction models for diagnosis and prognosis of covid-19 infection: systematic review and critical appraisal. *bmj* **2020**, *369*.
22. Ahmad, M.; Ahmed, I.; Jeon, G. An IoT-enabled real-time overhead view person detection system based on Cascade-RCNN and transfer learning. *Journal of Real-Time Image Processing* **2021**. https://doi.org/10.1007/s11554-021-01103-0.
23. shah, F.M.; Joy, S.K.S.; Ahmed, F.; Humaira, M.; Ami, A.S.; Paul, S.; Jim, A.R.K.; Hossain, T.; Ahmed, S. A Comprehensive Survey of COVID-19 Detection Using Medical Images **2020**. https://doi.org/10.31224/osf.io/9fdyp.
24. Wu, J.; Zhou, S.; Zuo, S.; Chen, Y.; Sun, W.; Luo, J.; Duan, J.; Wang, H.; Wang, D. U-Net combined with multi-scale attention mechanism for liver segmentation in CT images. *BMC Medical Informatics and Decision Making* **2021**, *21*, 1–12.
25. Ahmed, I.; Din, S.; Jeon, G.; Piccialli, F. Exploring deep learning models for overhead view multiple object detection. *IEEE Internet of Things Journal* **2019**, *7*, 5737–5744.
26. Wang, S.; Kang, B.; Ma, J.; Zeng, X.; Xiao, M.; Guo, J.; Cai, M.; Yang, J.; Li, Y.; Meng, X.; et al. A deep learning algorithm using CT images to screen for Corona Virus Disease (COVID-19). *MedRxiv* **2020**.
27. Hassanien, A.E.; Mahdy, L.N.; Ezzat, K.A.; Elmousalami, H.H.; Ella, H.A. Automatic x-ray covid-19 lung image classification system based on multi-level thresholding and support vector machine. *medRxiv* **2020**.
28. Kadry, S.; Rajinikanth, V.; Rho, S.; Raja, N.S.M.; Rao, V.S.; Thanaraj, K.P. Development of a Machine-Learning System to Classify Lung CT Scan Images into Normal/COVID-19 Class. *arXiv preprint arXiv:2004.13122* **2020**.
29. Hemdan, E.E.D.; Shouman, M.A.; Karar, M.E. Covidx-net: A framework of deep learning classifiers to diagnose covid-19 in x-ray images. *arXiv preprint arXiv:2003.11055* **2020**.
30. Wang, L.; Wong, A. COVID-Net: A Tailored Deep Convolutional Neural Network Design for Detection of COVID-19 Cases from Chest X-Ray Images. *arXiv preprint arXiv:2003.09871* **2020**.
31. Pathak, Y.; Shukla, P.K.; Tiwari, A.; Stalin, S.; Singh, S. Deep transfer learning based classification model for COVID-19 disease. *Irbm* **2020**.

32. Farooq, M.; Hafeez, A. Covid-resnet: A deep learning framework for screening of covid19 from radiographs. *arXiv preprint arXiv:2003.14395* **2020**.
33. Singh, D.; Kumar, V.; Kaur, M.; et al. Classification of COVID-19 patients from chest CT images using multi-objective differential evolution–based convolutional neural networks. *European Journal of Clinical Microbiology & Infectious Diseases* **2020**, *39*, 1379–1389.
34. Hossain, M.S.; Muhammad, G.; Guizani, N. Explainable AI and mass surveillance system-based healthcare framework to combat COVID-I9 like pandemics. *IEEE Network* **2020**, *34*, 126–132.
35. Muhammad, G.; Hossain, M.S. COVID-19 and non-COVID-19 classification using multi-layers fusion from lung ultrasound images. *Information Fusion* **2021**, *72*, 80–88.
36. Shorfuzzaman, M.; Hossain, M.S. MetaCOVID: A Siamese neural network framework with contrastive loss for n-shot diagnosis of COVID-19 patients. *Pattern recognition* **2021**, *113*, 107700.
37. Apostolopoulos, I.D.; Mpesiana, T.A. Covid-19: automatic detection from x-ray images utilizing transfer learning with convolutional neural networks. *Physical and Engineering Sciences in Medicine* **2020**, p. 1.
38. Pereira, R.M.; Bertolini, D.; Teixeira, L.O.; Silla Jr, C.N.; Costa, Y.M. COVID-19 identification in chest X-ray images on flat and hierarchical classification scenarios. *Computer Methods and Programs in Biomedicine* **2020**, p. 105532.
39. Ahmed, I.; Ahmad, A.; Jeon, G. An IoT based deep learning framework for early assessment of Covid-19. *IEEE Internet of Things Journal* **2020**, pp. 1–1. https://doi.org/10.1109/JIOT.2020.3034074.
40. Saeedi, A.; Saeedi, M.; Maghsoudi, A. A novel and reliable deep learning web-based tool to detect covid-19 infection from chest ct-scan. *arXiv preprint arXiv:2006.14419* **2020**.
41. Mobiny, A.; Cicalese, P.A.; Zare, S.; Yuan, P.; Abavisani, M.; Wu, C.C.; Ahuja, J.; de Groot, P.M.; Van Nguyen, H. Radiologist-level covid-19 detection using ct scans with detail-oriented capsule networks. *arXiv preprint arXiv:2004.07407* **2020**.
42. He, K.; Zhang, X.; Ren, S.; Sun, J. Deep residual learning for image recognition. In Proceedings of the Proceedings of the IEEE conference on computer vision and pattern recognition, 2016, pp. 770–778.
43. Song, Y.; Zheng, S.; Li, L.; Zhang, X.; Zhang, X.; Huang, Z.; Chen, J.; Wang, R.; Zhao, H.; Zha, Y.; et al. Deep learning enables accurate diagnosis of novel coronavirus (COVID-19) with CT images. *IEEE/ACM Transactions on Computational Biology and Bioinformatics* **2021**.
44. Zheng, C.; Deng, X.; Fu, Q.; Zhou, Q.; Feng, J.; Ma, H.; Liu, W.; Wang, X. Deep learning-based detection for COVID-19 from chest CT using weak label. *MedRxiv* **2020**.
45. Gozes, O.; Frid-Adar, M.; Greenspan, H.; Browning, P.D.; Zhang, H.; Ji, W.; Bernheim, A.; Siegel, E. Rapid ai development cycle for the coronavirus (covid-19) pandemic: Initial results for automated detection & patient monitoring using deep learning ct image analysis. *arXiv preprint arXiv:2003.05037* **2020**.
46. Jin, D.; Xu, Z.; Tang, Y.; Harrison, A.P.; Mollura, D.J. CT-realistic lung nodule simulation from 3D conditional generative adversarial networks for robust lung segmentation. In Proceedings of the International Conference on Medical Image Computing and Computer-Assisted Intervention. Springer, 2018, pp. 732–740.
47. Jiang, J.; Hu, Y.c.; Liu, C.J.; Halpenny, D.; Hellmann, M.D.; Deasy, J.O.; Mageras, G.; Veeraraghavan, H. Multiple resolution residually connected feature streams for automatic lung tumor segmentation from CT images. *IEEE transactions on medical imaging* **2018**, *38*, 134–144.
48. Wu, Y.H.; Gao, S.H.; Mei, J.; Xu, J.; Fan, D.P.; Zhang, R.G.; Cheng, M.M. Jcs: An explainable covid-19 diagnosis system by joint classification and segmentation. *IEEE Transactions on Image Processing* **2021**, *30*, 3113–3126.
49. Diniz, J.O.; Quintanilha, D.B.; Neto, A.C.S.; da Silva, G.L.; Ferreira, J.L.; Netto, S.M.; Araújo, J.D.; Da Cruz, L.B.; Silva, T.F.; Martins, C.M.d.S.; et al. Segmentation and quantification of COVID-19 infections in CT using pulmonary vessels extraction and deep learning. *Multimedia Tools and Applications* **2021**, pp. 1–33.
50. Qiu, Y.; Liu, Y.; Li, S.; Xu, J. Miniseg: An extremely minimum network for efficient covid-19 segmentation. *arXiv preprint arXiv:2004.09750* **2020**.
51. Müller, D.; Rey, I.S.; Kramer, F. Automated chest ct image segmentation of covid-19 lung infection based on 3d u-net. *arXiv preprint arXiv:2007.04774* **2020**.
52. Narin, A.; Kaya, C.; Pamuk, Z. Automatic detection of coronavirus disease (covid-19) using x-ray images and deep convolutional neural networks. *Pattern Analysis and Applications* **2021**, pp. 1–14.
53. Fan, D.P.; Zhou, T.; Ji, G.P.; Zhou, Y.; Chen, G.; Fu, H.; Shen, J.; Shao, L. Inf-net: Automatic covid-19 lung infection segmentation from ct images. *IEEE Transactions on Medical Imaging* **2020**, *39*, 2626–2637.
54. Ahmed, I.; Jeon, G.; Chehri, A. An IoT-enabled smart health care system for screening of COVID-19 with multi layers features fusion and selection. *Computing* **2022**, pp. 1–18.
55. Zhou, T.; Canu, S.; Ruan, S. Automatic COVID-19 CT segmentation using U-Net integrated spatial and channel attention mechanism. *International Journal of Imaging Systems and Technology* **2021**, *31*, 16–27.
56. Yang, J.; Qiu, K. An improved segmentation algorithm of CT image based on U-Net network and attention mechanism. *Multimedia Tools and Applications* **2021**, pp. 1–24.
57. Oktay, O.; Schlemper, J.; Folgoc, L.L.; Lee, M.; Heinrich, M.; Misawa, K.; Mori, K.; McDonagh, S.; Hammerla, N.Y.; Kainz, B.; et al. Attention u-net: Learning where to look for the pancreas. *arXiv preprint arXiv:1804.03999* **2018**.
58. Kervadec, H.; Bouchtiba, J.; Desrosiers, C.; Granger, E.; Dolz, J.; Ayed, I.B. Boundary loss for highly unbalanced segmentation. In Proceedings of the International conference on medical imaging with deep learning. PMLR, 2019, pp. 285–296.

59. Virtanen, P.; Gommers, R.; Oliphant, T.E.; Haberland, M.; Reddy, T.; Cournapeau, D.; Burovski, E.; Peterson, P.; Weckesser, W.; Bright, J.; et al. SciPy 1.0: fundamental algorithms for scientific computing in Python. *Nature methods* **2020**, *17*, 261–272.
60. Schlemper, J.; Oktay, O.; Schaap, M.; Heinrich, M.; Kainz, B.; Glocker, B.; Rueckert, D. Attention gated networks: Learning to leverage salient regions in medical images. *Medical image analysis* **2019**, *53*, 197–207.
61. Zhou, Z.; Rahman Siddiquee, M.M.; Tajbakhsh, N.; Liang, J. Unet++: A nested u-net architecture for medical image segmentation. In *Deep learning in medical image analysis and multimodal learning for clinical decision support*; Springer, 2018; pp. 3–11.
62. Yin, S.; Deng, H.; Xu, Z.; Zhu, Q.; Cheng, J. SD-UNet: A Novel Segmentation Framework for CT Images of Lung Infections. *Electronics* **2022**, *11*, 130.